Nanoscale

ROYAL SOCIETY OF CHEMISTRY

PAPER

View Article Online
View Journal | View Issue

Cite this: *Nanoscale*, 2024, **16**, 16919

Role of additive size in the segmental dynamics and mechanical properties of cross-linked polymers†

Xiangrui Zheng,[a] Lan Xu,[b] Jack F. Douglas *[c] and Wenjie Xia *[b]

Thermoset materials often involve the addition of molecular and nanoparticle additives to alter various chemo-physical properties of importance in their ultimate applications. The resulting compositional heterogeneities can lead to either enhancement or degradation of thermoset properties, depending on the additive chemical structure and concentration. We tentatively explore this complex physical phenomenon through the consideration of a model polymeric additive to our coarse-grained (CG) thermoset investigated in previous works by simply varying the size of additive segments compared to those of polymer melt. We find that the additive modified thermoset material becomes chemically heterogeneous from additive aggregation when the additive segments become much smaller than those of the thermoset molecules, and a clear evidence is observed in the spatial distribution of local molecular stiffness estimated from Debye–Waller factor $\langle u^2 \rangle$. Despite the non-monotonic variation trends observed in dynamical and mechanical properties with decreasing additive segmental size, both the structural relaxation time and moduli (*i.e.*, shear modulus and bulk modulus) exhibit scaling laws with $\langle u^2 \rangle$. The present work highlights the complex role of additive size played in the dynamical and mechanical properties of thermoset polymers, which should provide a better understanding for the glass formation process of cross-linked polymer composites.

Received 25th June 2024,
Accepted 13th August 2024

DOI: 10.1039/d4nr02631d

rsc.li/nanoscale

1. Introduction

Cross-linked polymers have been widely used in various applications due to their light weight, superior mechanical properties, and thermal and chemical stability.[1,2] However, for some cross-linked polymers, their normally highly cross-linked nature results in some inherent disadvantages, such as brittleness, poor fatigue resistance and low impact resistance, which severely impedes their further applications.[3] The introduction of additives provides a promising strategy to tune the dynamics and mechanical properties of cross-linked polymers.[4–7] For example, plasticizers reduce the glass transition temperature (T_g) and improve the flexibility and ductility of polymers,[8–10] while anti-plasticizer additives normally result in a decrease in T_g and the fragility of glass formation, but an increase in the stiffness of polymer material to which they are added in the glassy state.[11,12]

Numerous previous studies have indicated the addition of additives provides a promising strategy to tune the mechanical properties of polymers based on the additive distribution in the polymer matrix. In particular, the introduction of additives into epoxy resins could efficiently improve the fracture toughness, impact resistance and heat stability of cross-linked polymers by the phase separation occurred at the micro and nanoscale.[13–19] As an specific example, Zhang and coworkers systematically investigated the influence of frequently used thermoplastics, such as hydroxyl terminated polyethersulfone (PES),[3] polysulfone (PSF)[14] and polyetherketone cardo (PEK-C),[20] on the phase morphology and mechanical properties of epoxy resin. With the increasing content of thermoplastics, the phase structure of blends presented uniformly dispersed particles, bi-continuous and phase inverted structures, where the greatest enhancement effect in the fracture toughness and impact strength were obtained in epoxy/ther-

[a]Department of Mechanics, School of Aerospace Engineering, Huazhong University of Science and Technology, Wuhan, 430074, China
[b]Department of Aerospace Engineering, Iowa State University, Ames, Iowa 50011, USA. E-mail: wxia@iastate.edu
[c]Materials Science and Engineering Division, National Institute of Standards and Technology, Gaithersburg, Maryland 20899, USA. E-mail: jack.douglas@nist.gov

†Electronic supplementary information (ESI) available: Thermodynamical properties (Fig. S1), the effect of cross-link density (Fig. S2), the definition of Debye–Waller factor $\langle u^2 \rangle$ (Fig. S3), the polymer–additive interfacial interaction (Fig. S4) and the determination of bulk modulus (Fig. S5). See DOI: https://doi.org/10.1039/d4nr02631d

moplastic blends with a bi-continuous phase structure. Apart from the toughening effect, the additives also showed potential for tuning the microstructure of epoxy resin. Recently, Zhao *et al.*[21] introduced fumed silica into epoxy resin to fine control the microstructure of polymer blends by phase separation, where the structure of epoxy resin was improved to form a porous material with smaller pore size as the content of fumed silica increased, and at the same time, the fumed silica could be removed without affecting the matrix and skeleton structure of the porous material.

Even if there is no phase separation between polymer matrix and additives, varying the additive chemical structure,[9,22,23] concentration,[24–26] size,[27–29] stiffness[30–32] and the polymer–additive interaction strength,[24,33,34] can also influence the relaxation dynamics and mechanical properties of thermoset materials. In particular, additive size can exert a complex influence on the performances of glass-forming polymers. Cheng *et al.*[35] systematically compared the effect of nanoparticle size on the structural dynamics of poly(2-vinylpyridine) where the T_g and fragility of glass formation were found to exhibit dramatic changes with the increasing concentration of attractive nanoparticles having a size on the order of the polymer segments, while only small property changes were found when SiO_2 additive particles having a diameter of 25 nm were added. Ash and coworkers[36] investigated how the size of alumina nanoparticles influenced the mechanical properties of poly(methyl methacrylate), where the introduction of relatively large 38 nm alumina nanoparticles resulted in a brittle-to-ductile transition of the composite thermoset material in uniaxial tension, along with an increase in the strain of failure. On the other hand, 17 nm additives showed similar brittle behavior as neat poly(methyl methacrylate). It is notable that the smaller 17 nm additives tended to aggregate, so that these particles could not be uniformly dispersed. Finally, experiments performed by Serenko *et al.*[37] indicated that the aggregation of rigid polyphenylene dendrimers caused degraded polymer properties in comparison to the pure polymer material.[38,39] It is evidently important to better understand the relationship between additive size and additive–polymer matrix interaction on phase separation and the influence of additive phase separation on the thermodynamical, dynamical and mechanical properties of polymers in order to improve the functional performance of cross-linked polymer materials.

Compared to experiments, computational simulations provide details at a molecular scale that can be helpful in developing and understanding structure–property relationships of complex polymer materials, although the inherent limited simulation timescale can be a serious drawback in practice. For example, the increased local shear modulus in the vicinity of nanoparticle surface indicated that there was a glassy layer surrounding the nanoparticle, and the shear modulus of the glassy layer gradually decreased as the particle size got smaller.[27] Recent molecular dynamics (MD) simulations performed by Starr and coworkers[40,41] also demonstrated that the length scale of interfacial zone describing the range of altered dynamics around model nanoparticle additives decreased with the decreasing nanoparticle size at a strong interfacial interaction. Apart from nanoparticle additives, Zirdehi *et al.*[28,29] found that altering the segment size of model polymeric additive molecules over a wide range had a significant effect on the relaxation dynamics of polymeric and other model glass-forming materials, in which the relaxation time at low temperatures and characteristic temperatures of glass formation both exhibited a non-monotonic dependence on the additive segment size at a fixed additive concentration. They speculated that the non-monotonic size-effect might be attributed to the local packing efficiency and coupling of the dynamics between the polymer matrix and additives. A similar non-monotonic variation in relaxation time of coarse-grained (CG) polymer melts with spherical particle additives having a range of sizes was observed recently by McKenzie-Smith and coworkers,[42] where the relaxation time of polymer melts was well-described by the localization model (LM) emphasizing average molecular displacements on a picosecond timescale, *i.e.*, "dynamic free volume". In addition, MD simulations on binary mixtures of particles having different sizes have previously indicated that a large size ratio of particles promoted a tendency towards phase separation.[43,44] In view of these observations on how varying particle or additive segment size affects the performances of polymer matrix,[36,37,45,46] we infer that varying the segment size of molecular additives could induce significant alterations in mechanical and dynamical properties even when the polymer-matrix interaction strength is relatively attractive as consequence of the normally low entropy of mixing of polymer materials. Such an effect can be expected to be particularly large when there is a large asymmetry in the additive and matrix bead sizes. We thus arrive at a simple CG model for exploring the influence of additive size on the glass-forming properties of thermoset materials with additives.

In our pervious works,[47–49] we systematically investigated the influence of cross-link density, cohesive interaction strength and chain stiffness on the relaxation dynamics and

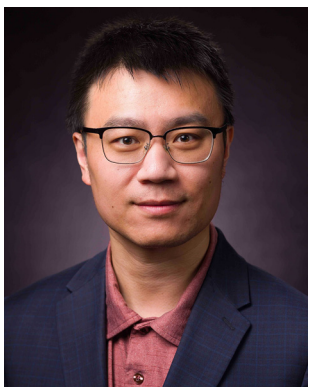

Wenjie Xia

Dr Wenjie Xia is an Associate Professor in the Department of Aerospace Engineering at Iowa State University. He earned his Ph.D. from Northwestern University in 2016. Dr Xia's research expertise lies in the multiscale modeling and computational design of polymers and soft matter, with a particular emphasis on understanding and predicting the complex behaviors of multifunctional and structural materials.

mechanical properties of pure cross-linked polymers using CG-MD simulation, where qualitative trends were found to accord rather well with experiments on thermoset materials.[50–52] Recent MD simulations on the glass formation of cross-linked polymer/additive mixtures having a wide range of cross-link densities indicated that introduction of additives can lead to a decrease in the characteristic temperatures and fragility of glass formation, and these changes are often accompanied by significant changes in the material moduli.[53]

Considering the practical significance of additives on the mechanical properties of thermoset materials, we systematically explore the structure, structural relaxation dynamics and mechanical properties for glass-forming cross-linked polymers with polymeric additives having variable additive segment size, but a fixed concentration to keep the simulations within manageable proportions. The findings of our exploratory study provide key physical insights into how additive segment size affects the segmental dynamics and mechanical properties of cross-linked polymer materials. This knowledge should be helpful in arriving at a better control of molecular parameters of real thermoset materials.

2. Model and simulation details

2.1 Coarse-grained (CG) model

The molecular models of cross-linked polymer and additives are represented by a widely used bead-spring model in the CG-MD simulations on glass-forming polymers.[54] The cross-linked polymer is composed of 686 linear chains with a chain length of 15 beads and 343 tetra-functional star cross-linkers. In addition, 200 linear additive molecules consisting of 15 beads with varying bead size are introduced into the system, *i.e.*, the mass fraction of additive particles defined as the ratio of the mass of additive particles to the total mass of particles in the polymer/additives mixture is kept constant at ~20%. The linear chains, cross-linkers and additives are initially randomly mixed in a large simulation box with periodic boundary conditions in all directions (Fig. 1).

The non-bonded interactions are represented by the standard truncated and shifted Lennard-Jones (LJ) potential,

$$U_{\mathrm{LJ}}(r) = \begin{cases} 4\varepsilon\left[\left(\frac{\sigma}{r}\right)^{12} - \left(\frac{\sigma}{r}\right)^{6} - \left(\frac{\sigma}{r_c}\right)^{12} + \left(\frac{\sigma}{r_c}\right)^{6}\right], & r < r_c \\ 0, & r \geq r_c \end{cases} \quad (1)$$

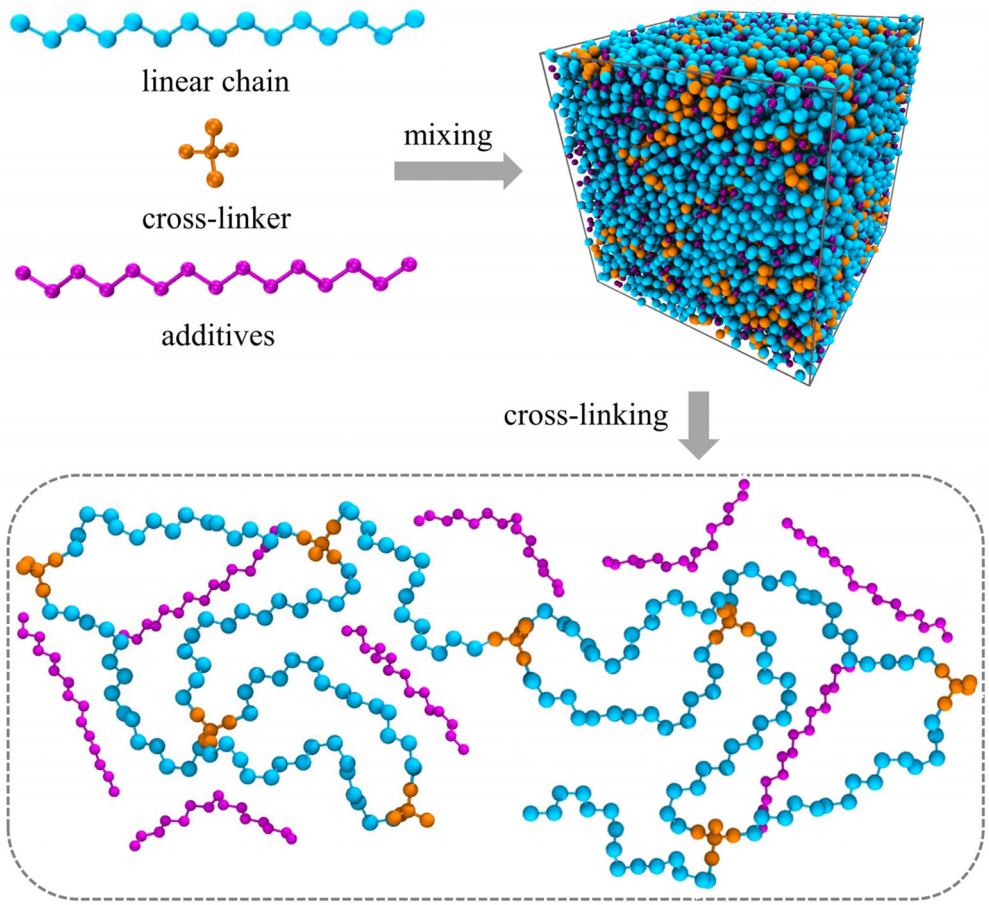

Fig. 1 The molecular structures of linear chain (cyan beads), cross-linker (orange beads) and additive (purple beads). The molecules are homogenously mixed in an amorphous simulation box with periodic boundary conditions. Subsequently, the linear chains and cross-linkers are cross-linked to a polymer network.

where r is the distance between two beads, $r_c = 2.5\sigma$ is the cutoff distance, σ governs the effective van der Waals radius, and ε describes the cohesive energy strength of the cross-linked polymers and additives. To investigate the effect of segment size of additive on the glass formation of cross-linked polymers, the bead size of cross-linked polymers σ_p is fixed at 1.0σ, while the bead size of additives σ_a varies from 0.3σ to 1.0σ, and the σ_{ap} in the additive–polymer interaction is defined as the average of σ_p and σ_a following the standard Lorentz rule. The cohesive interaction strengths for additive–additive and polymer–polymer are chosen to be 1.0ε, while the cohesive energy between additive and polymer is set to be 1.5ε to promote enthalpically dispersed state.[42] The bond connectivity along neighbouring beads is maintained *via* the harmonic spring potential,

$$U_{\text{harm}}(r) = \frac{1}{2}k_b(r - r_0)^2 \quad (2)$$

where the force strength $k_b = 2000\varepsilon/\sigma^2$ and the equilibrium bond length $r_0 = 0.97\sigma$, which is chosen to avoid crystallization and form an amorphous material.[55,56] The bending constraint is modeled by a simple cosine angular potential,[57,58]

$$U_{\text{bend}}(\theta) = k_\theta[1 + \cos(\theta)] \quad (3)$$

where the bending strength $k_\theta = 0.2\varepsilon$ representing a relatively flexible chain, θ is the angle composed of three consecutive bonded particles. All the quantities are expressed in the standard reduced LJ unit for convenience. The basic quantities, including length σ, energy ε and mass of each bead m, and other units of interest, can be derived from these fundamental units. For example, time τ, temperature T and pressure P can be described in units of $\tau_{LJ} = (m\sigma^2/\varepsilon)^{1/2}$, $T = \varepsilon/k_B$ and $P = \varepsilon/\sigma^3$, respectively. The thermodynamic, segmental dynamics, and mechanical properties of thermoset material with molecular additives are next analyzed following exactly the same procedures as considered previously for the pure thermoset materials.[47–49]

2.2 Simulation details

All the MD simulations were performed in large scale atomic/molecular massively parallel simulator (LAMMPS) software.[59] The mixture of linear chains, cross-linkers and additives were first relaxed in a constant-pressure and constant-temperature (NPT) ensemble at a high temperature $T = 1.5\varepsilon/k_B$ and a pressure $P = 0.0\varepsilon/\sigma^3$ for $t = 10^4\tau_{LJ}$ to ensure that the linear chains, cross-linkers and additives were homogenously mixed. Then, the mixture was progressively cooled down to $T = 1.0\varepsilon/k_B$ over a period of $t = 10^4\tau_{LJ}$. Finally, the system was equilibrated at $T = 1.0\varepsilon/k_B$ in NPT ensemble for $t = 2 \times 10^4\tau_{LJ}$, following a canonical (NVT) ensemble for $t = 10^4\tau_{LJ}$. Subsequently, a cross-linking and multiple relaxation algorithm proposed by Varshney *et al.*[60] was utilized to cross-link the linear chains and cross-linkers into a polymer network, which has successfully captured the thermodynamics and mechanical properties of highly cross-linked polymers.[60–62] The end beads in linear chains and cross-linkers were set as the reactive beads, which could form new chemical bonds, where the stoichiometric ratio of reactive beads in linear chains and cross-linkers was 1 : 1. When the distance of two end beads located in linear chains and cross-linkers respectively was less than 1.3σ, a new covalent bond was introduced between the two beads. Then a NPT relaxation was performed at $T = 1.0\varepsilon/k_B$ over a period of $t = 5 \times 10^3\tau_{LJ}$ to reduce the energy fluctuations resulted by the new formed covalent bonds. The cross-link density defined as the ratio of reacted end beads to the total number of ends beads of linear chains was 94% for the final cross-linked polymers.

Three models were independently established and cross-linked to get rid of the effect of configuration and cross-linked structure. After cross-linking the polymer, we systematically modified the additives size in the cross-linked polymer/additive mixtures varying from 0.3σ to 1.0σ in order to investigate the effect of additive size, while the additives mass fraction, polymer–additives interaction strength parameter ε_{ap} and cross-link density of cross-linked polymer were all fixed. The mixtures were first relaxed using NPT ensemble at a high temperature $T = 2.0\varepsilon/k_B$, while the pressure varied in the range from $10.0\varepsilon/\sigma^3$ to $0.0\varepsilon/\sigma^3$ for two cycles over a period of $10^4\tau_{LJ}$. Then, the cross-linked polymer/additive mixtures with varying additive size were sufficiently relaxed at a constant pressure $P = 0.0\varepsilon/\sigma^3$ for $t = 2 \times 10^4\tau_{LJ}$ in NPT ensemble, followed by a NVT relaxation over a period of $10^4\tau_{LJ}$. For the equilibrated systems, a quenching process from a high temperature $T = 2.0\varepsilon/k_B$ to a low temperature $T = 0.1\varepsilon/k_B$ in a stepwise fashion with a temperature step size of $\Delta T = 0.05\varepsilon/k_B$ was performed. At each temperature, the polymers were successively relaxed in NPT ensemble for $t = 2 \times 10^4\tau_{LJ}$ and in NVT ensemble for $10^4\tau_{LJ}$, then the configurations were collected at the end of each run. The mixture systems with different additive bead size are denoted as $\sigma_a = x$, which means that the bead size of additives is x in the corresponding cross-linked polymer/additive mixture model.

3. Results and discussion

3.1 Thermodynamical properties

We first analyze the influence of additive size on the fundamental thermodynamical properties, including density ρ, reduced thermal expansion coefficient α_p^* and dimensionless isothermal compressibility κ_T^*, which are summarized in Fig. S1 in the ESI.† Compared to pure cross-linked polymer without any additives, the introduction of additives leads to an increase in ρ and a slight decrease in α_p^* and κ_T^*. Additives with smaller bead size result in a remarkably large ρ but a similar α_p^* and κ_T^* as the pure polymer.

Besides the basic thermodynamical properties, the static structure factor characterizing the material "structure" in terms of local density variations is measured at $T = 1.0\varepsilon/k_B$ for cross-linked polymer/additive mixtures with a wide range of additive bead size. The static structure factor $S(q)$, which

describes the mean correlations in the positions of segments, is defined as,

$$S_\alpha(q) = \frac{1}{N}\left\langle \sum_{j\in\alpha}^{N_\alpha}\sum_{k\in\alpha}^{N_\alpha} \exp[-i\boldsymbol{q}\cdot(\boldsymbol{r}_j - \boldsymbol{r}_k)] \right\rangle \quad (4)$$

where α denotes the species of particles (*i.e.*, $S_m(q)$ denotes $S(q)$ of the whole cross-linked polymer and additive mixtures, $S_p(q)$ denotes partial $S(q)$ of polymer–polymer in mixtures, and $S_a(q)$ denotes partial $S(q)$ of additives-additives in mixtures), $i = \sqrt{-1}$, $q = |\boldsymbol{q}|$ is the wavenumber, $\boldsymbol{r}_j$ is the coordinate of particle j, and $\langle\ldots\rangle$ denotes the usual thermal average. The additive segment size exhibits an obvious influence on the position and amplitude of the first peak of $S_m(q)$ for cross-linked polymer/additives mixtures (Fig. 2a). The wavenumber at which $S_m(q)$ reaches its first peak shows a non-monotonic variation with the decreasing additive size, where the wavenumber decreases gradually with the increasing bead size for bead size larger than 0.6σ, while a reasonably opposed trend is observed for smaller bead size (see right inset of Fig. 2a). The additive having a similar relative bead size leads to an increase in the amplitude of first peak of $S_m(q)$, while smaller bead size reduces the amplitude of $S_m(q)$ obviously. In addition, the introduction of additives with bead size $\sigma_a = 0.3\sigma$ results in a large increase in $S_m(q)$ at the limit of q close to 0 (see the left inset of Fig. 2a), which may be related to additive aggregation resulted from the large asymmetry between the cross-linked polymer and additive bead sizes. Sanz *et al.*[63] investigated the impact of fullerene on the structure of polystyrene–fullerene mixtures using small angle neutron scattering experiments, where the scattering intensity at low wavenumber remarkably increased as the fullerene agglomeration increasing with increasing fullerene concentration. Similarly, Banerjee *et al.*[64] observed large composition fluctuations in the region of sufficiently small q at low temperatures in Kob–Andersen mixtures consistent with phase separation. The time-resolved light scattering and X-ray scattering experiments also indicated that the scattering intensity increased continuously from the beginning of phase separation.[65–67]

The partial static structure factor curves of polymer–polymer in polymer/additives mixtures, $S_p(q)$, with a wide range of additive segment size is reasonably consistent with the pure polymer melt, and only a small difference in $S_p(q)$ at small q for mixtures with additive bead size larger than 0.8σ is observed (Fig. 2b). The similar $S_p(q)$ curves indicate that the additive aggregation induced by altering bead size of additive would not remarkably affect the local density fluctuations of polymer–polymer part in polymer/additives mixtures.[42] Similarly, Zirdehi *et al.*[28] analyzed the partial radial pair distribution functions for glass-forming polymer materials in the presence of additives with various bead sizes, which was directly related to the static structure factor. They found that the additive size had a negligible influence on the monomer–monomer pair distribution functions, but an obvious effect on the monomer–additive and additive–additive pair distribution functions, in accord with Fig. 2.

3.2 Dynamical properties

Next, we explore the influence of additive size on the relaxation dynamics based on the structural relaxation time τ_α. τ_α is determined from the time at which the self-part of intermediate scattering function $F_s(q, t)$ measuring the correlation of positions of polymer segments with time evolution decays to 0.2,

$$F_s(q,t) = \frac{1}{N}\left\langle \sum_{j=1}^{N} \exp\{-i\boldsymbol{q}\cdot[\boldsymbol{r}_j(t) - \boldsymbol{r}_j(0)]\} \right\rangle \quad (5)$$

where the wavenumber $q = |\boldsymbol{q}|$ is chosen to be the position of the first peak of $S(q)$ for our polymer/additive mixtures with varying additive segment size (right inset of Fig. 2a), and $\boldsymbol{r}_j(t)$

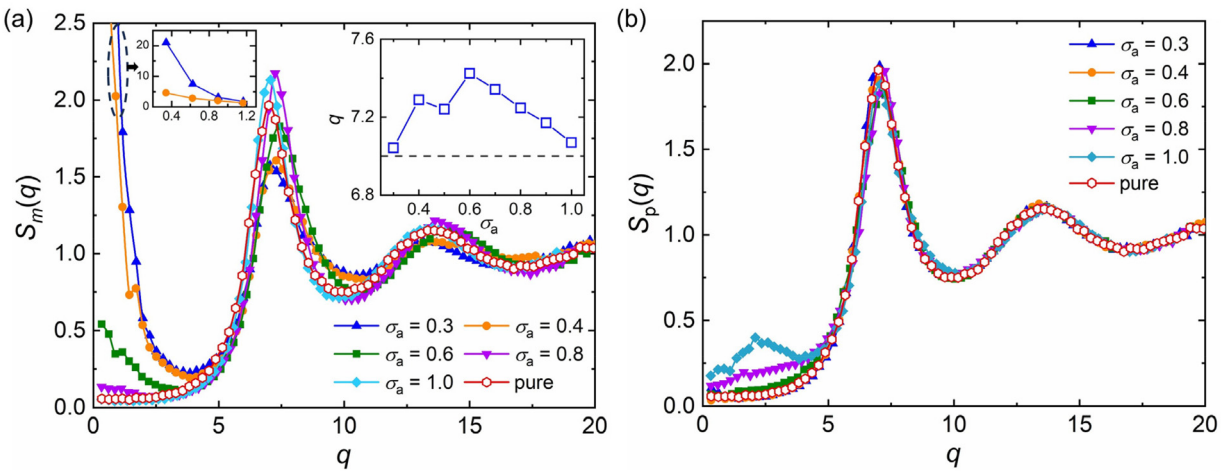

Fig. 2 The static structure factor $S(q)$ at $T = 1.0\varepsilon/k_B$ for pure polymer and polymer/additive mixtures with varying additive bead size σ_a. (a) The $S_m(q)$ of polymer/additive mixtures. The right inset descripts the wavenumber at which $S_m(q)$ reaches its first peak, where the dashed line shows the first peak position of pure polymer. The left inset describes $S_m(q)$ at the limit of q close to 0 for systems with small additive segment size. (b) Partial $S_p(q)$ of polymer–polymer in polymer/additive mixtures.

is the coordinate of particle j at the time t. The average is over all beads and over distinct starting times.

Fig. 3a summarizes the τ_α as a function of $1/T$ for mixtures with a wide range of additive segment size, where τ_α increases significantly upon cooling as observed in various glass-forming liquids.[68–71] The introduction of polymer additives having a segment size that is no larger than those of polymer particles results in a remarkable slowing down in the structural relaxation dynamics for cross-linked polymer/additive mixtures, as observed by McKenzie-Smith *et al.* in the linear polymer melts with nanoparticle additives.[42] A strong slowing down in relaxation dynamics was also demonstrated by Cheng *et al.*[35] using broadband dielectric spectroscopy when nanoparticles with nearly equivalent size to the polymer segments were progressively added into the poly(2-vinylpyridine) polymer. Whereas, a faster relaxation dynamic was reported in linear polymer/additive mixtures upon introducing additives with varying bead size, where the additives were represented by single spherical particles and the interaction strength in additive–polymer, additive–additive and polymer–polymer were identical.[28]

The relaxation time of polymer/additive mixtures shows a non-monotonic dependence on the additive size,[28,29] and we further analyze the effect of bead size on the relaxation time of polymer/additive mixtures in Fig. 3b. The polymer/additive mixture with additive bead size $\sigma_a = 0.8\sigma$ exhibits the slowest relaxation dynamics, and the relaxation time of polymer/additive mixtures (open symbols) and the partial relaxation time of cross-linked polymer in mixtures (solid symbols) progressively decrease when the bead size is larger or smaller than the critical size 0.8σ. The difference in the relaxation time between pure polymer without additives and polymer/additive mixtures is substantially reduced with the decreasing additive bead size.[40] In addition, there is no obvious difference in the relaxation time of polymer/additive mixtures (open symbols) and the partial relaxation time of cross-linked polymer in mixtures (solid symbols) when additive bead size is larger than 0.4σ, while the cross-linked polymer part in mixtures exhibits obviously faster relaxation dynamics than the whole polymer/additive mixtures for mixtures with additive aggregation (*i.e.*, $\sigma_a \leq 0.3\sigma$), indicating a remarkable slowing down of the dynamics arising from the molecular additive. The similar trends are also observed in cross-linked polymer/additive mixtures with lower cross-link densities (Fig. S2 in the ESI†), where decreasing cross-link density of polymer leads to faster relaxation dynamics for the whole mixtures and part of cross-linked polymer. This variability in the segmental dynamics could be altered by varying the intermolecular interaction strength between polymer and additives.[42] Hence, we emphasize that the trend observed is only limited for the range of bead size investigated, CG models of cross-linked polymer and additives, and intermolecular interaction strength used in the present work. The effect of a wider range of bead size on the relaxation dynamics for cross-linked polymers with varying intermolecular interaction strength and cross-link density deserves a systematical study in the future.

Numerous experiments and simulation works have previously demonstrated that the structural relaxation time of broadly glass-forming liquids follows Arrhenius law at high temperature, while a non-Arrhenius regime is observed below the onset temperature.[34,51,69,70] Here, we examine the validity of non-Arrhenius regime for τ_α at low T based on the Vogel–Fulcher–Tammann (VFT) relation, $\ln(\tau_\alpha/\tau_0) = DT_0/(T - T_0)$. In particular, the Vogel temperature T_0 at which the relaxation time τ_α extrapolates to infinity characterizes the end of glass transition process, and the kinetic fragility parameter $K = 1/D$, describes the steepness of T-dependence of τ_α near glass transition temperature T_g. The inset of Fig. 3a shows that the T-dependent relaxation time follows the VFT relation for mixtures at their glassy states, which indicates that the VFT

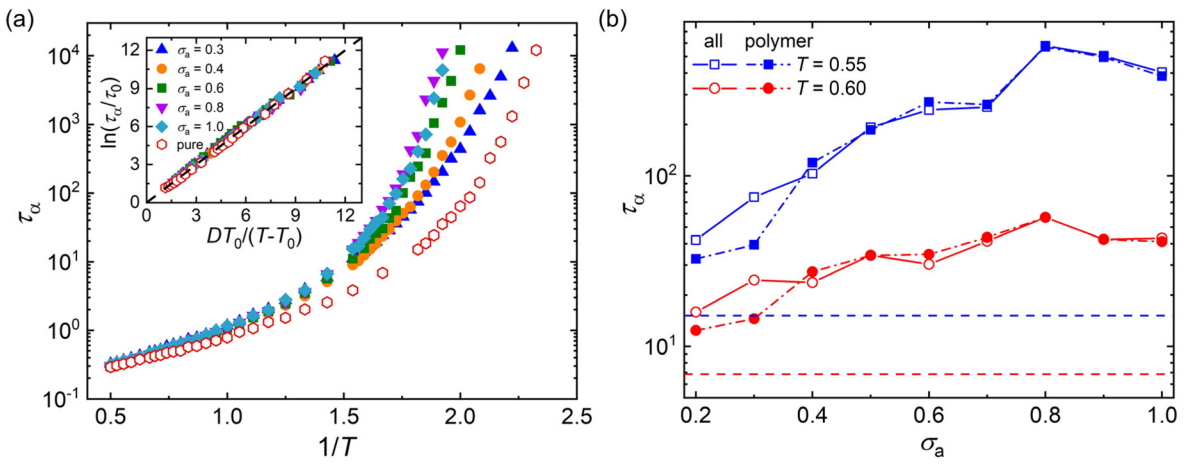

Fig. 3 (a) The structural relaxation time τ_α as a function of $1/T$ for polymer/additive mixtures with varying additive bead size σ_a. The inset descripts the VFT collapse of T-dependence of τ_α for various σ_a for mixtures at their glassy states. Dashed line indicates the VFT relation, $\ln(\tau_\alpha/\tau_0) = DT_0/(T - T_0)$. (b) τ_α as a function of σ_a for polymer/additive mixtures (open symbols) and partial τ_α of polymer (solid symbols) in polymer/additive mixtures. The dashed lines indicate τ_α of the pure polymer without additives.

relation can describe the segmental relaxation behaviors at low T well for cross-linked polymer/additive mixtures with a wide range of additive bead size.

To avoid extrapolation in the simulation estimates of T_g, T_g here is defined by the temperature at which τ_α reaches to $10^3\tau_{LJ}$ which we refer to as the "computational T_g".[31] This T_g estimation is significantly different in magnitude, but seems to vary nearly proportionately to the T_g determined from the empirical definition often utilized in experiments, *i.e.*, $\tau_\alpha(T_g)$ = 100*s* or the "kink temperature" in the variation of density with T at a much slower cooling rate than that utilized in our simulations.[32,47,50] The results of Fig. 4a indicate that both T_g and T_0 show a non-monotonic variation with the decreasing additive size. Additives having a similar size as the polymer segmental size ($\sigma_a = 0.8\sigma$ and $\sigma_a = 1.0\sigma$) result in significant increases in T_g and T_0, while these characteristic temperatures of glass formation gradually decrease for additives having a size smaller than the polymer segments. The slower relaxation dynamics and an increase in T_g were also observed in poly(2-vinylpyridine) with the introduction of oligomeric nanoparticle with a diameter indentical to the polymer segment size, and the increase amplitude of T_g became larger when the additive concentration increased.[35]

It is notable that the additives having a bead size identical to the polymer segments exhibit a similar fragility parameter K with the pure polymer (Fig. 4b). Similar to the characteristic temperatures, the fragility of mixtures decreases progressively with decreasing bead size of additives for additives with smaller bead size than those of polymer matrix. Thus, compared with the pure polymer without any additives, the introduction of additives having a smaller bead size than the polymer segments leads to an increase in T_g, but a decrease in fragility for polymer/additive mixtures. Apart from the kinetic fragility parameter K, the characteristic temperature ratio, a measure of temperature width of glass transition, is also often used to characterize the degree of T-dependence of τ_α for polymeric glass-formers.[11,24,70] A larger T_0/T_g is observed with increasing additive size until $\sigma_a = 0.8\sigma$ (inset of Fig. 4b), indicating a narrower temperature width of glass transition and thus a more fragile glass former. The characteristic temperature ratio T_0/T_g exhibits a consistent variation trend with the kinetic fragility parameter K, as observed in a wide range of polymers and their nanocomposites.[24,56,70]

Except for the structural relaxation time τ_α, the mean-square displacement (MSD) of segments is also calculated to further explore the effect of additive bead size on the dynamics at the timescale of picosecond for polymer/additive mixtures. The Debye–Waller parameter $\langle u^2\rangle$ is determined from the MSD at $t = 1\tau_{LJ}$ for pure polymer and polymer/additive mixtures with varying additive bead size (Fig. S3 in the ESI†). As shown in Fig. 5a, the pure polymer exhibits a larger $\langle u^2\rangle$ over a wide range of temperatures than $\langle u^2\rangle$ of the polymer/additive mixtures, indicating a faster dynamic for pure cross-linked polymer, qualitatively consistent with the trend observed in τ_α. Desai *et al.*[72] found that the chain diffusion coefficient, another mobility measure, showed an obvious decrease relative to that in the pure polymer when the polymer–nanoparticle interactions were strongly attractive. We infer that the slower segmental dynamics in polymer/additive mixtures may be ascribed to the strongly attractive interaction between polymer and additives, where an acceleration in dynamics of polymer mixtures was observed for an identical or weaker polymer–additive interaction strength.[28,73] In addition, the mobility of mixtures exhibits slight variation with the additive size for additives with size larger than 0.4σ. The inset of Fig. 5a analyzes the effect of additive bead size on the $\langle u^2\rangle$ of mixtures and the part of additives in detail. The average mobility of additives (open symbols) progressively increases with the decreasing bead size of additives, except an unexpected reduction in additive mobility for $\sigma_a = 0.3\sigma$ at a low temperature ($T = 0.5\varepsilon/k_B$). With the additive bead size decreasing, the

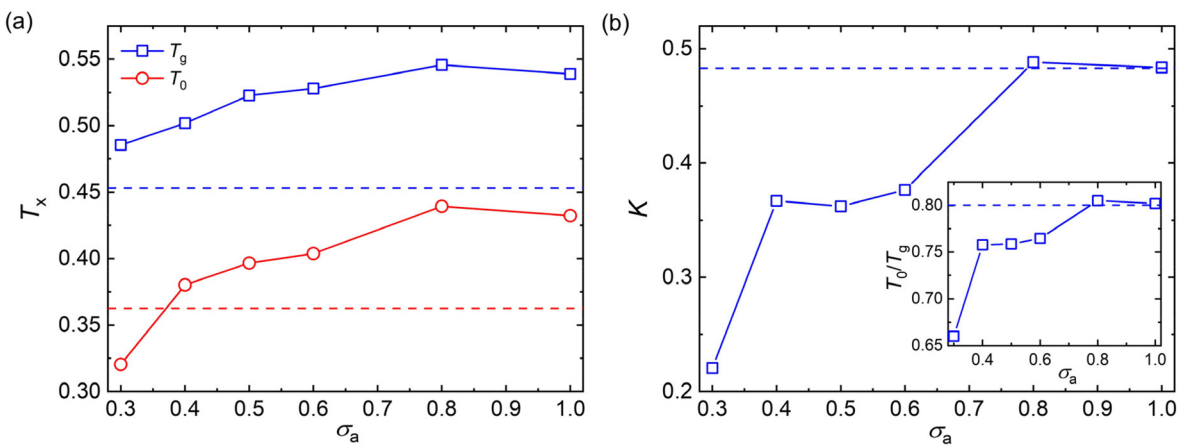

Fig. 4 (a) The glass transition temperature T_g (blue square) and Vogel temperature T_0 (red circle) for polymer/additive mixtures with varying additives bead size σ_a. The colored dashed lines descript the corresponding temperature of pure polymer without any additives. (b) The fragility parameter K as a function of σ_a for polymer/additive mixtures. The inset descripts the characteristic temperature ratio T_0/T_g. The dashed lines descript the value of pure polymer.

molecular mobility of additives increases progressively. At the same time, the decreasing additive size also leads to a decrease in the interaction strength between additive and cross-linked polymer (Fig. S4 in the ESI†), which results in the occurrence of additive aggregation for mixtures with sufficiently small additive size ($\sigma_a = 0.3\sigma$). The additive aggregation further decreases the additive mobility significantly, leading to a reduction in the Debye–Waller factor of additives. Thus, a non-monotonic variation in $\langle u^2 \rangle$ is observed at low temperatures.

The effect of temperature on $\langle u^2 \rangle$ is further explored in Fig. 5b. When the additive bead size is identical to polymer beads (*i.e.*, $\sigma_a = 1.0\sigma$), the whole mobility of mixtures (solid symbols) is always faster than the part of additives (open symbols), indicating faster dynamics of cross-linked polymer part than the additives in the mixtures. However, an opposing trend is observed in the mixtures with $\sigma_a = 0.4\sigma$. Consistently, a smaller τ_α is observed in the part of cross-linked polymer than that of the whole polymer/additive mixtures for $\sigma_a = 1.0\sigma$, while the cross-linked polymer part exhibits a larger τ_α for mixtures with $\sigma_a = 0.4\sigma$ (see Fig. 3b). As the additive bead size decreases to 0.3σ, the whole mixture has a slower mobility than the additives for T larger than $0.8\varepsilon/k_B$, consistent with that observed in the mixtures with $\sigma_a = 0.4\sigma$. And the difference of mobility between cross-linked polymer and additives gets larger with increasing T. When the T is cooled down below $0.8\varepsilon/k_B$, a weakly faster mobility is observed in mixtures, contrary to that observed in high T.

Despite the large timescale difference between segmental relaxation and particle vibration, it has long been recognized that there are correlations between high and low frequency response.[74–76] Until now, different theoretical models were developed to understand the correlation of structural relaxation time and rattling amplitude for glass formers in their glassy state.[77–79] For example, Simmons and coworkers[79] developed a localization model to describe the scaling law between structural relaxation time τ_α and Debye–Waller factor $\langle u^2 \rangle$ based on a dynamical free volume argument,

$$\tau_\alpha = \tau_0 \exp[(u_0^2/\langle u^2 \rangle)^{\alpha/2}] \quad (6)$$

where τ_0, u_0^2 and a are fitting parameters, and the parameter α reflects the anisotropic shape of local free volume. In particular, the volume $\langle u^2 \rangle^{3/2}$ explored by a spherical particle in the glass-forming liquid was interpreted as "dynamical free volume",[74] and α values different from 3 were correspondingly interpreted in terms of anisotropic "rattle volumes" on a caging timescale explored by molecules of more complex shape. Despite the sucessful application of the localization model (LM) to various glass-forming materials,[79–81] the model remains a semi-empirical model. The fundamental origin of the scaling law between $\langle u^2 \rangle$ and τ_α remains incompletely understood.

Here, we examine the scaling relationship between $\langle u^2 \rangle$ and τ_α for polymer/additive mixtures with a wide range of additive bead size using the LM, where the exponent α is fixed as 3 (Fig. 6a). It can be seen that the LM (dashed line) can describe the scaling law between $\langle u^2 \rangle$ and τ_α well for pure polymer and polymer/additive mixtures with various additive bead sizes, which demonstrates that there are indeed close correlation between fast β relaxation dynamics occuring at the timescale of ps and structural relaxation occurring on a much longer timescale. The fitting parameters τ_0 and u_0^2 are summarized in Fig. 6b. Both τ_0 and u_0^2 exhibited a non-monotonic variation with the additive bead size, where an extremum value was reasonably observed at $\sigma_a = 0.8\sigma$. For additives with bead size smaller than 0.8σ, the τ_0 gradually decreased while u_0^2 roughly increased with the increasing bead size of additives, consistent with the trends observed in linear polymer melts with variable additive size and polymer–additive interaction strength.[42] In

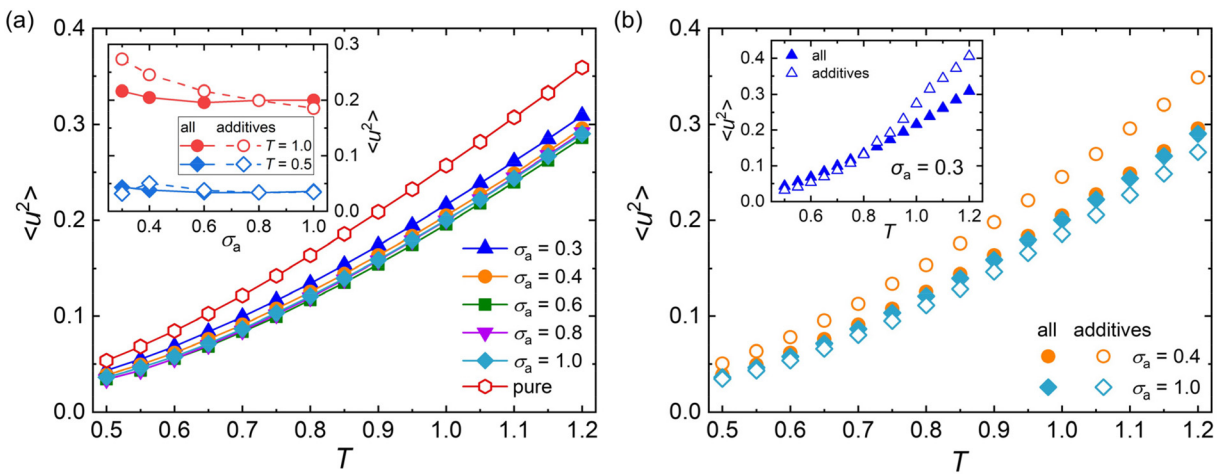

Fig. 5 (a) The Debye–Waller factor $\langle u^2 \rangle$ over a wide range of temperature T for polymer/additive mixtures with varying additives bead size σ_a. The inset descripts $\langle u^2 \rangle$ as a function of σ_a for polymer/additive mixtures and the part of additives at different T. (b) $\langle u^2 \rangle$ as a function of T for polymer/additive mixtures with varying σ_a. The inset descripts $\langle u^2 \rangle$ for polymer/additive mixtures with $\sigma_a = 0.3\sigma$.

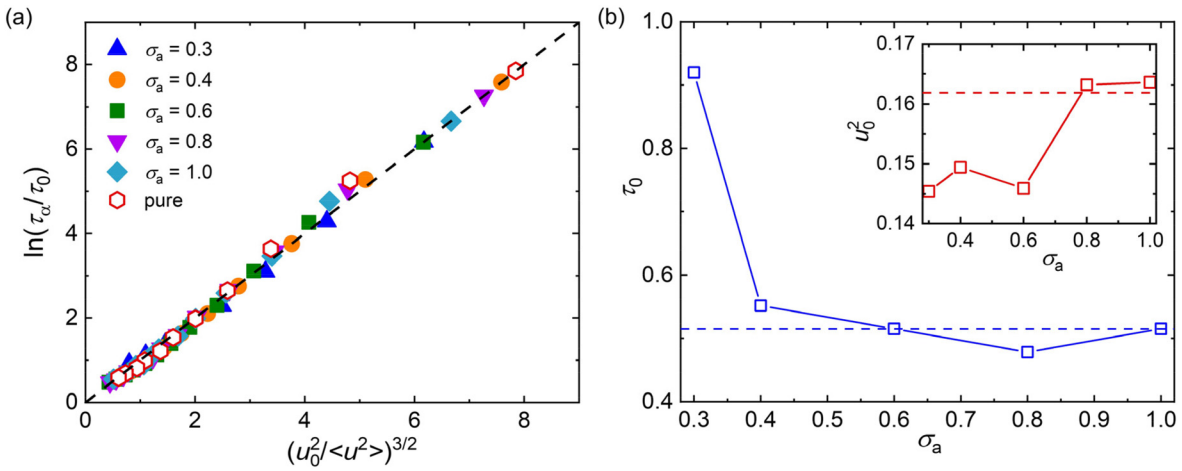

Fig. 6 (a) Tests of the localization model predictions (dashed line) for pure polymer and polymer/additive mixtures with varying additives size σ_a. The data show a good collapse onto the localization model. (b) The fitting parameters τ_0 and u_0^2 as a fucntion of σ_a. The dashed lines are the fitting parameters of pure polymer.

addition, Pazmiño Betancourt *et al.*[80] found that the exponent α was approximately equal to 3 for polymer nanocomposites with varying nanoparticle concentrations and for polymer thin films with a wide range of thickness, as in the original computational study of τ_α *versus* $\langle u^2\rangle$ for pure polymer melt by Starr *et al.*[74] Similarly, a series of works on the metallic and polymeric glass formers also indicated that the exponent α might be a constant near 3.[42,81,82] However, Simmons *et al.*[83] later found that α was apparently material-dependent due to the presence of caging anisotropy as suggested in the LM[79] and the presence of anharmonic intermolecular interactions. Later simulations further seemed to indicate that α depends on chain stiffness,[31,49,84] material cooling rate,[85] and cross-link density,[47] providing additional evidence that the fundamental origin of the relation between τ_α and $\langle u^2\rangle$ is uncertain.

3.3 Mechanical properties

It has long been recognized that the introduction of plasticizers would efficiently increase the flexibility of glassy polymers, while the anti-plasticizers usually increase the stiffness of polymers in their glassy state.[12,86] Here, we analyze the effect of additive bead size on the shear modulus over a wide range of temperatures for cross-linked polymer/additive mixtures in their glassy state, which is essential in the engineering applications. The shear deformation tests are performed independently for five times for each system with a strain rate of $5 \times 10^{-4}\tau_{LJ}^{-1}$, and the shear modulus G is calculated from the linear regime of shear stress–strain curves.

Compared to pure polymer, the introduction of additives with a wide range of bead size leads to a significant increase in the shear modulus for a strongly attractive interaction between polymer and additives (Fig. 7a), in good agreement with the addition of attractive nanoparticles into linear polymer melts.[27] The bead size of additives has a remarkable non-monotonic influence on the shear modulus of polymer/additive mixtures, where the inset of Fig. 7a summarizes the influence of additive bead size on the shear modulus of mixtures at two different temperatures. For the bead size of additives larger than 0.6σ, the shear modulus of mixtures roughly increases with the decreasing additive bead size. Whereas, the shear modulus G suddenly decreases when the bead size decreased to 0.3σ, which may be attributed to the occurence of additive aggregation resulted from the progressively decrease of additive–polymer interaction strength (Fig. S4 in the ESI†). Thus, the shear modulus of mixtures exhibits a non-monotonic trend with the decreasing additive size. A similar variation trend is also observed in the bulk modulus B for mixtures in their glassy state (Fig. S5 in the ESI†), where the bulk modulus is calculated from the reciprocal of isothermal compressibility. Numerous experiments have demonstrated that the phase separation could remarkably enhance the toughness of epoxy, but would reduce the modulus and strength with various degrees at the same time.[13–15,18]

Apart from the scaling law between $\langle u^2\rangle$ and τ_α, the mechanical properties, such as shear modulus, Young's modulus, bulk modulus and Poisson ratio, were all found to have correlation with the Debye–Waller parameter $\langle u^2\rangle$.[87–90] In our previous works,[47–49] we have observed the linear scaling relationship between shear modulus and $\langle u^2\rangle$ for pure cross-linked polymers with a wide range of cross-link densities, cohesive interaction strength and chain stiffness and for polymer/additive mixtures with varying additive mass percentage.[53] Here, we examine the validity of the scaling law between shear modulus and $\langle u^2\rangle$ for polymer/additive mixtures with varying additive bead size in Fig. 7b. It can be seen that a reasonably linear relationship between shear modulus G and $k_BT/\langle u^2\rangle$ is again observed for polymer/additive mixtures with a wide range of additive bead size, regardless of whether there is additive aggregation within the mixtures. The scaling law has been observed in a wide range of metallic and polymeric glass formers.[89–91] Most recently, Xu *et al.*[92] also reported the same linear relationship between the glassy plateau shear modulus

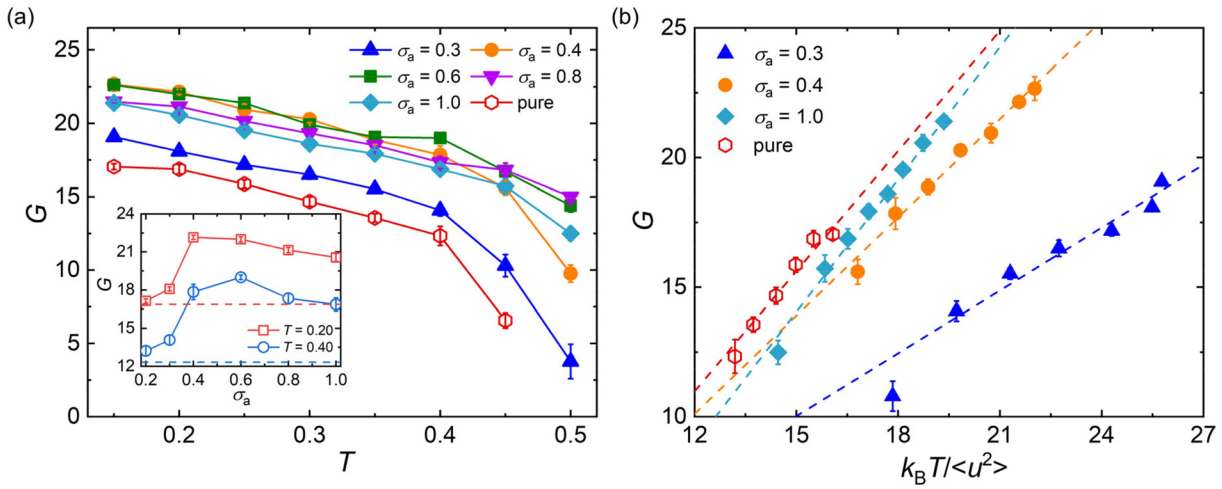

Fig. 7 The glassy shear modulus G for pure polymer and polymer/additive mixtures with varying additives size σ_a. (a) G as a function of temperature T. The inset descripts G as a function of σ_a. (b) G as a function of local molecular stiffness $k_BT/\langle u^2\rangle$. The dashed lines indicate the linear fitting.

and Debye–Waller parameter for linear polymer melts with variable pressure, chain stiffness and chain length. Except for the shear modulus, the bulk moduli of pure cross-linked polymer and its mixtures also exhibit a scaling law with $\langle u^2\rangle$ (Fig. S5b in ESI†).[93] In view of the close relationship between material moduli and the Debye–Waller parameter, $k_BT/\langle u^2\rangle$ is often termed as "local molecular stiffness".[91,93]

3.4 Elastic heterogeneity

The atomistic MD simulation on the cross-linked poly(dicyclopentadiene) networks demonstrated that the atoms in linear segments exhibited a remarkably higher mobility than those in cross-links.[94] Similarly, the simulation work on the glass-forming polymers also indicated that the mobility of particles was heterogeneous, where the particle clusters could be extremely immobile or mobile.[11,12,95] Based on the analyses of local molecular stiffness $k_BT/\langle u^2\rangle$, an extremely immobile cluster usually corresponds to a stiff region, while the particles with high mobility would lead to a local softness.[87,91] Hence, the dynamical heterogeneity resulted from the difference in particle mobility also termed as "elastic heterogeneity". The shear band formation of Zr–Cu metallic glasses was found to initiate at the local soft regions, where the particles had a larger $\langle u^2\rangle$ describing the atomic displacement on a caging timescale.[91]

Fig. 8 shows the probability density distribution of local molecular stiffness $k_BT/\langle u^2\rangle$ at a low temperature $T = 0.5\varepsilon/k_B$, in order to explore the role of additive size played in the elastic heterogeneity for polymer/additive mixtures. The probability density function of $k_BT/\langle u^2\rangle$ of pure polymer without any additives (red curves) exhibits a Gaussian form, as observed in cross-linked polymers with and without bending constraints.[47–49] The addition of additives leads to an obviously wider distribution than the slender shape observed in pure polymer, indicating a greater degree of elastic heterogeneity in polymer/additive mixtures. With the decreasing bead size of additives, the shape of probability distribution gradually

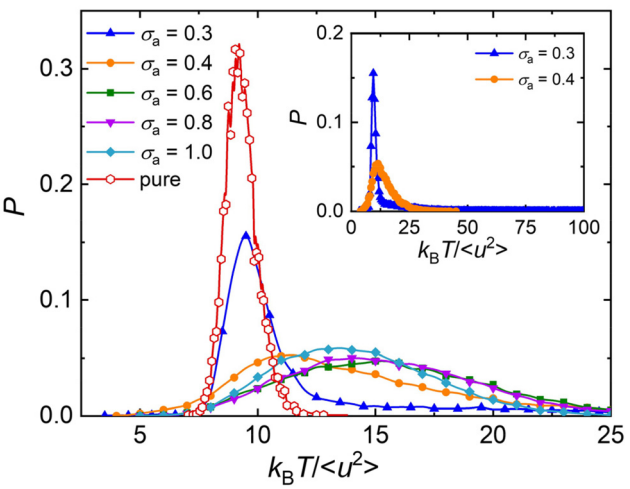

Fig. 8 The probability density distribution of local stiffness $k_BT/\langle u^2\rangle$ at $T = 0.5\varepsilon/k_B$ for pure polymer and polymer/additive mixtures with varying additives size σ_a. The inset descripts the entire distribution of $k_BT/\langle u^2\rangle$ for mixtures with $\sigma_a = 0.3\sigma$ and $\sigma_a = 0.4\sigma$.

departs from the Gaussian form and exhibits a log–normal distribution, along with the occurrence of a long tail. It is notable that there is an extremely long tail for polymer/additive mixture with additive bead size $\sigma_a = 0.3\sigma$ (inset of Fig. 8), which may be related to the sudden increase in the static strcture factor at low wavenumber. We infer that the additive aggregation results in the occurence of local extremely stiff regions, and thus leads to a long tail in the large $k_BT/\langle u^2\rangle$. Consistent with the ditribution of local stiffness in our present work, de Pablo and coworkers also found that the local shear moduli of polymeric glasses were inhomogeneous, and the elastic heterogeneity increased with decreasing nanoparticle size.[27] In addition, the width of local stiffness distribution decreases reasonably for the polymer/additive mixtures with

smaller additive bead size, corresponding to a stronger glass former. A similar relationship between fragility and width of local stiffness distribution was observed before in our pure cross-linked polymer having the same monomer structure as that used in the present work, but having a variable cross-link density[47] and chain bending stiffness.[49] However, Xu *et al.*[96] recently reported the opposite trend in star polymer melts with varying number of star arms in which the stronger glass former exhibited a broader local stiffness distribution. This kind of opposed correlation fragility and the breath of the local stiffness distribution has also observed in our pure cross-linked polymer melts with varying cohesive interaction strength.[48] Unfortunately, there appears to be no general trend between the breath of local stiffness fluctuations (an attractive and concrete measure of dynamic heterogeneity) and the fragility.

We further analyze the spatial distribution of $k_BT/\langle u^2\rangle$ of mixtures and additives in an attempt to obtain a better intuitive understanding of elastic heterogeneity and its physical significance. Fig. 9 shows the spatial distribution of $k_BT/\langle u^2\rangle$ at $T = 0.5\varepsilon/k_B$, where the red domains in the color map correspond to relatively stiff regions while teal blue domains indicate regions having a relatively low local stiffness. The color bar scale is the same for all the systems in order to make direct comparisons of the local stiffness of materials. The polymer/additive mixtures obviously exhibit more stiff regions (red domains) and more remarkable variation in local stiffness than pure polymer, indicating a stiffer material and a greater degree of local elastic heterogeneity, consistent with the variation of shear modulus and probability distribution of local molecular stiffness. The influence of additives on the local elastic properties is reminiscent of anti-plasticizers, which would lead to an increase in the moduli and a larger amplitude of fluctuations in local elastic constants compared to pure polymer.[11,12] As the bead size of additives decreases from 1.0σ to 0.6σ, the average value of local moelcular stiffness and the degree of elastic heterogeneity both increase remarkably. When the bead size of additives further decreased to 0.4σ, the molecular stiffness slightly decreases along with a relatively well-distributed local stiffness. However, a large stiff (red) region is observed, while other regions are relatively soft (teal blue) for mixtures with $\sigma_a = 0.3\sigma$. We infer that the significant decrease in shear modulus of the entire material may be ascribed to the agglomeration of immobile particles.[39]

Fig. 10 further explores the spatial distribution of local stiffness of additives for mixtures with $\sigma_a = 0.3\sigma$ and $\sigma_a = 0.4\sigma$ at $T = 0.5\varepsilon/k_B$, where the symbol size and color both describe the value of local stiffness indicating important heterogeneity in moelcular stiffness, and the symbol position represents the actual positions of additives in the mixtures. The additives with small bead size (*i.e.*, $\sigma_a = 0.3\sigma$) exhibit obvious lower molecular mobility than those with bead size $\sigma_a = 0.4\sigma$. According to the spatial distribution of additives, the additives in the polymer/additive mixture with $\sigma_a = 0.3\sigma$ tend to aggregate in agreement with the huge increment of $S(q)$ at q close to 0, which resulted in significant reduction in the elastic modulus of mixtures. In contrast, the additives are evenly distributed in the mixture with $\sigma_a = 0.4\sigma$. As the bead size disparity between cross-linked polymer and additives increases, the small size of additives promotes the occurence of aggregation within the polymer.[39] Similarly, Nie *et al.* observed the emergence of phase separation in binary mixtures of soft particles with big

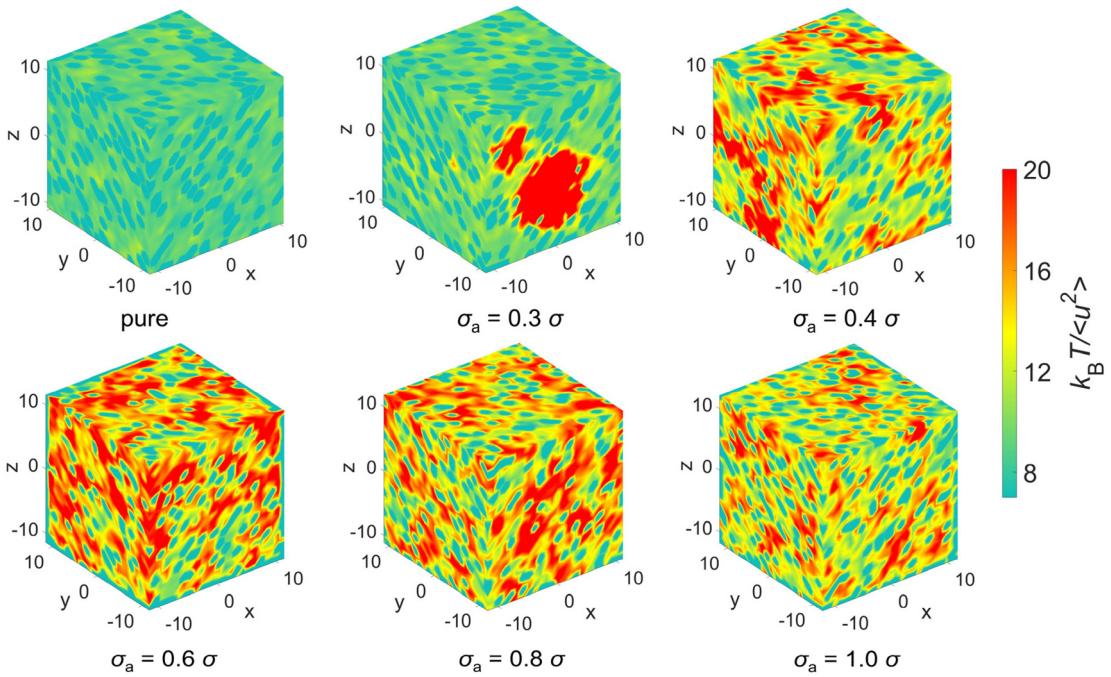

Fig. 9 The spatial distribution of local stiffness $k_BT/\langle u^2\rangle$ at $T = 0.5\varepsilon/k_B$ for pure polymer and polymer/additive mixtures with varying additives size σ_a.

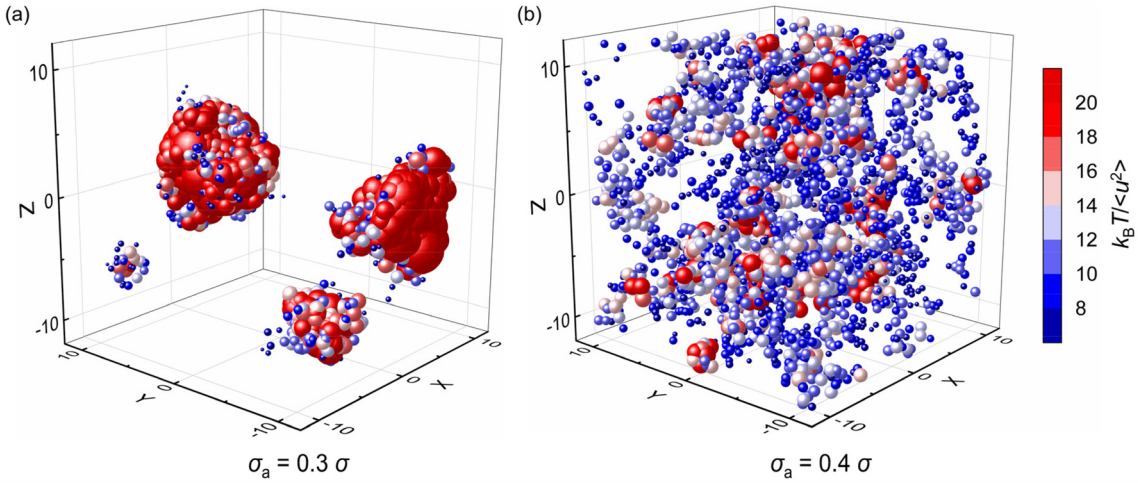

Fig. 10 The spatial distribution of local stiffness $k_BT/\langle u^2\rangle$ of additives for polymer/additive mixtures with additives bead size $\sigma_a = 0.3\sigma$ and $\sigma_a = 0.4\sigma$. The color and size both indicate the value of $k_BT/\langle u^2\rangle$. The position descripts the actual coordinates of additives in the mixtures. The color bar is the same for all plots. In particular, the additives are aggregated in figure (a), while they are nearly evenly distributed in (b).

size disparity over a wide range of pressure and quench rate.[43] Hence, in order to better improve the mechanical properties of cross-linked polymers, it is essential to make a reasonable choice of additive size to aviod additive agglomeration.

4. Conclusions

In the present work, we have systematically explored the effect of additive segmental size on the dynamical and mechanical properties of cross-linked polymers using a bead-spring CG model of thermoset polymer and molecular additive. The introduction of polymer additives having a wide range of bead sizes was found to lead to a significant influence on thermodynamic and dynamic properties of the thermoset material. The comparison of structural relaxation time τ_α demonstrates that when the additives have higher attraction strength with polymer than the additive–additive and polymer–polymer interaction strength, the relaxation dynamics of polymer/additive mixtures significantly slows down, along with a larger characteristic temperature (*i.e.*, glass transition temperature T_g and Vogel temperature T_0) and a smaller fragility of glass formation compared to the pure polymer without additives. The structural relaxation time, characteristic temperatures and fragility of glass formation all exhibit a non-monotonic dependence on the bead size of additives, where they reach their maximum values at the additive bead size $\sigma_a = 0.8\sigma$. A similar non-monotonic vairation is also observed in the variation of Debye–Waller factor $\langle u^2\rangle$ and shear modulus G over a wide range of temperatures. It is notable that both τ_α and G exhibit scaling laws with $\langle u^2\rangle$ for polymer/additive mixtures with variable additive bead size, consistent with that widely observed in polymeric and metallic glass formers. In addition, the spatial distribution of local moelcular stiffness calculated from $\langle u^2\rangle$ also indicates that such additives tend to aggregate when the bead size is sufficiently small. The observations of the present work provide physical insights into how the additive size influences the dynamical and mechanical properties of cross-linked polymers, which should be helpful in the rational design of cross-linked polymer materials.

Author contributions

Xiangrui Zheng: conceptualization, software, formal analysis, methodology, investigation, writing – original draft and writing – review & editing; Lan Xu: methodology, formal analysis, review & editing; Jack F. Douglas: conceptualization, supervision, and writing – editing & review; Wenjie Xia: conceptualization, supervision, resources, and writing – editing & review.

Data availability

All the data that support the findings of this study are included within the article (and the ESI†).

Conflicts of interest

There are no conflicts to declare.

Acknowledgements

X. Z. acknowledges the support from the Postdoctoral Fellowship Program of CPSF (grant no. GZB20230242). The computation is completed in the HPC Platform of Huazhong University of Science and Technology. L. X. and

W. X. acknowledge the support from the Department of Aerospace Engineering at Iowa State University.

References

1 Y. Gao, K. Peng and S. Mitragotri, *Adv. Mater.*, 2021, **33**, 2006362.
2 Y. Tang, W. Xu, S. Niu, Z. Zhang, Y. Zhang and Z. Jiang, *J. Mater. Chem. A*, 2021, **9**, 10000–10011.
3 M. Jiang, Y. Liu, C. Cheng, J. Zhou, B. Liu, M. Yu and H. Zhang, *Polym. Test.*, 2018, **69**, 302–309.
4 G. D. Vilakati, E. M. V. Hoek and B. B. Mamba, *Polym. Test.*, 2014, **34**, 202–210.
5 D. Mathew, C. P. Reghunadhan Nair and K. N. Ninan, *J. Appl. Polym. Sci.*, 2000, **77**, 75–88.
6 T. C. Merkel, B. D. Freeman, R. J. Spontak, Z. He, I. Pinnau, P. Meakin and A. J. Hill, *Science*, 2002, **296**, 519–522.
7 A. L. Andrady, T. C. Merkel and L. G. Toy, *Macromolecules*, 2004, **37**, 4329–4331.
8 M. W. Halloran, J. A. Nicell, R. L. Leask and M. Marić, *J. Appl. Polym. Sci.*, 2022, **139**, e52778.
9 M. H. Baghersad, A. Habibi and A. Heydari, *J. Mol. Struct.*, 2017, **1130**, 447–454.
10 K. Kawai and Y. Hagura, *Carbohydr. Polym.*, 2012, **89**, 836–841.
11 R. A. Riggleman, J. F. Douglas and J. J. de Pablo, *J. Chem. Phys.*, 2007, **126**, 234903.
12 R. A. Riggleman, J. F. Douglas and J. J. de Pablo, *Soft Matter*, 2010, **6**, 292–304.
13 V. S. Mathew, C. Sinturel, S. C. George and S. Thomas, *J. Mater. Sci.*, 2010, **45**, 1769–1781.
14 Z. Sun, L. Xu, Z. Chen, Y. Wang, R. Tusiime, C. Cheng, S. Zhou, Y. Liu, M. Yu and H. Zhang, *Polymers*, 2019, **11**, 461.
15 Y. Liu, W. Zhang and H. Zhou, *Polym. Int.*, 2005, **54**, 1408–1415.
16 H. Chen, Z. Zhu, D. Patil, D. Bajaj, N. Verghese, Z. Jiang and H.-J. Sue, *Polymer*, 2023, **270**, 125763.
17 M. I. Calafel, E. Calahorra, P. M. Remiro and M. Cortazar, *Colloid Polym. Sci.*, 2010, **288**, 1281–1291.
18 L. Dong, W. Zhou, X. Sui, Z. Wang, H. Cai, P. Wu, J. Zuo and X. Liu, *J. Electron. Mater.*, 2016, **45**, 3776–3785.
19 H. Deng, L. Yuan, A. Gu and G. Liang, *J. Appl. Polym. Sci.*, 2020, **137**, 48394.
20 S. Zhou, Z. Chen, R. Tusiime, C. Cheng, Z. Sun, L. Xu, Y. Liu, M. Jiang, J. Zhou, H. Zhang and M. Yu, *Compos. Commun.*, 2019, **13**, 80–84.
21 J. Zhao, J. Wang, Z. Liu, Y. Zhang and Y. Mi, *ACS Appl. Polym. Mater.*, 2023, **5**, 2859–2866.
22 X. H. Flora, M. Ulaganathan and S. Rajendran, *Int. J. Polym. Mater.*, 2013, **62**, 737–742.
23 A. Taghizadeh, P. Sarazin and B. D. Favis, *J. Mater. Sci.*, 2013, **48**, 1799–1811.
24 F. W. Starr and J. F. Douglas, *Phys. Rev. Lett.*, 2011, **106**, 115702.
25 R. A. Riggleman, K. Yoshimoto, J. F. Douglas and J. J. de Pablo, *Phys. Rev. Lett.*, 2006, **97**, 045502.
26 R. A. Riggleman, J. F. Douglas and J. J. de Pablo, *Phys. Rev. E: Stat., Nonlinear, Soft Matter Phys.*, 2007, **76**, 011504.
27 G. J. Papakonstantopoulos, M. Doxastakis, P. F. Nealey, J.-L. Barrat and J. J. de Pablo, *Phys. Rev. E: Stat., Nonlinear, Soft Matter Phys.*, 2007, **75**, 031803.
28 E. M. Zirdehi and F. Varnik, *J. Chem. Phys.*, 2019, **150**, 024903.
29 E. M. Zirdehi, T. Voigtmann and F. Varnik, *J. Phys.: Condens. Matter*, 2020, **32**, 275104.
30 Y. Zhu, A. Giuntoli, W. Zhang, Z. Lin, S. Keten, F. W. Starr and J. F. Douglas, *J. Chem. Phys.*, 2022, **157**, 094901.
31 J. H. Mangalara and D. S. Simmons, *ACS Macro Lett.*, 2015, **4**, 1134–1138.
32 J. H. Mangalara, M. D. Marvin, N. R. Wiener, M. E. Mackura and D. S. Simmons, *J. Chem. Phys.*, 2017, **146**, 104902.
33 B. A. Pazmiño Betancourt, J. F. Douglas and F. W. Starr, *Soft Matter*, 2013, **9**, 241–254.
34 S.-J. Li, H.-J. Qian and Z.-Y. Lu, *Soft Matter*, 2019, **15**, 4476–4485.
35 S. Cheng, S.-J. Xie, J.-M. Y. Carrillo, B. Carroll, H. Martin, P.-F. Cao, M. D. Dadmun, B. G. Sumpter, V. N. Novikov, K. S. Schweizer and A. P. Sokolov, *ACS Nano*, 2017, **11**, 752–759.
36 B. J. Ash, R. W. Siegel and L. S. Schadler, *Macromolecules*, 2004, **37**, 1358–1369.
37 O. A. Serenko, V. I. Roldughin, A. A. Askadskii, E. S. Serkova, P. V. Strashnov and Z. B. Shifrina, *RSC Adv.*, 2017, **7**, 50113–50120.
38 P. Lepcio, F. Ondreas, K. Zarybnicka, M. Zboncak, O. Caha and J. Jancar, *Soft Matter*, 2018, **14**, 2094–2103.
39 W. Xia, X. Qin, Y. Zhang, R. Sinko and S. Keten, *Macromolecules*, 2018, **51**, 10304–10311.
40 H. Emamy, S. K. Kumar and F. W. Starr, *Phys. Rev. Lett.*, 2018, **121**, 207801.
41 W. Zhang, H. Emamy, B. A. Pazmiño Betancourt, F. Vargas-Lara, F. W. Starr and J. F. Douglas, *J. Chem. Phys.*, 2019, **151**, 124705.
42 T. Q. McKenzie-Smith, J. F. Douglas and F. W. Starr, *Phys. Rev. Lett.*, 2021, **127**, 277802.
43 Y. Nie, J. Liu, J. Guo and N. Xu, *Nat. Commun.*, 2020, **11**, 3198.
44 M. Dijkstra, R. van Roij and R. Evans, *Phys. Rev. Lett.*, 1998, **81**, 2268–2271.
45 P. S. Anbinder, P. J. Peruzzo and J. I. Amalvy, *Prog. Org. Coat.*, 2016, **101**, 207–215.
46 A. Karuth, S. Szwiec, G. M. Casanola-Martin, A. Khanam, M. Safaripour, D. Boucher, W. Xia, D. C. Webster and B. Rasulev, *Prog. Org. Coat.*, 2024, **193**, 108526.
47 X. Zheng, Y. Guo, J. F. Douglas and W. Xia, *J. Chem. Phys.*, 2022, **157**, 064901.
48 X. Zheng, Y. Guo, J. F. Douglas and W. Xia, *Macromolecules*, 2022, **55**, 9990–10004.
49 X. Zheng, W. Nie, Y. Guo, J. F. Douglas and W. Xia, *Macromolecules*, 2023, **56**, 7636–7650.

50 B. Mei, T.-W. Lin, G. S. Sheridan, C. M. Evans, C. E. Sing and K. S. Schweizer, *Macromolecules*, 2022, **55**, 4159–4173.
51 Y. Kashiwagi, O. Urakawa, S. Zhao, Y. Takashima, A. Harada and T. Inoue, *Macromolecules*, 2021, **54**, 3321–3333.
52 A. J. Lesser and K. J. Calzia, *J. Polym. Sci., Part B: Polym. Phys.*, 2004, **42**, 2050–2056.
53 W. Nie, J. F. Douglas and W. Xia, *ACS Eng. Au*, 2023, **3**, 512–526.
54 K. Kremer and G. S. Grest, *J. Chem. Phys.*, 1990, **92**, 5057–5086.
55 W.-S. Xu, J. F. Douglas and K. F. Freed, *Macromolecules*, 2016, **49**, 8341–8354.
56 W.-S. Xu, J. F. Douglas and K. F. Freed, *Macromolecules*, 2016, **49**, 8355–8370.
57 D. Pan and Z.-Y. Sun, *J. Chem. Phys.*, 2018, **149**, 234904.
58 A. Shavit and R. A. Riggleman, *Macromolecules*, 2013, **46**, 5044–5052.
59 A. P. Thompson, H. Metin Aktulga, R. Berger, D. S. Bolintineanu, W. Michael Brown, P. S. Crozier, P. J. in't Veld, A. Kohlmeyer, S. G. Moore, T. D. Nguyen, R. Shan, M. J. Stevens, J. Tranchida, C. Trott and S. J. Plimpton, *Comput. Phys. Commun.*, 2022, **271**, 108171.
60 V. Varshney, S. S. Patnaik, A. K. Roy and B. L. Farmer, *Macromolecules*, 2008, **41**, 6837–6842.
61 A. Bandyopadhyay, P. K. Valavala, T. C. Clancy, K. E. Wise and G. M. Odegard, *Polymer*, 2011, **52**, 2445–2452.
62 A. Shokuhfar and B. Arab, *J. Mol. Model.*, 2013, **19**, 3719–3731.
63 A. Sanz, H. C. Wong, A. J. Nedoma, J. F. Douglas and J. T. Cabral, *Polymer*, 2015, **68**, 47–56.
64 A. Banerjee, M. Sevilla, J. F. Rudzinski and R. Cortes-Huerto, *Soft Matter*, 2022, **18**, 2373–2382.
65 G. Shen, Z. Hu, Z. Liu, R. Wen, X. Tang and Y. Yu, *RSC Adv.*, 2016, **6**, 34120–34130.
66 Z. Xia, W. Li, J. Ding, A. Li and W. Gan, *J. Polym. Sci., Part B: Polym. Phys.*, 2014, **52**, 1395–1402.
67 G. Li, Z. Huang, C. Xin, P. Li, X. Jia, B. Wang, Y. He, S. Ryu and X. Yang, *Mater. Chem. Phys.*, 2009, **118**, 398–404.
68 B. Mei, Y. Zhou and K. S. Schweizer, *Macromolecules*, 2021, **54**, 10086–10099.
69 D. M. Duarte, W. Tu, A. Dzienia and K. Adrjanowicz, *Polymer*, 2019, **183**, 121860.
70 X. Xu, J. F. Douglas and W.-S. Xu, *Macromolecules*, 2021, **54**, 6327–6341.
71 Z. Yang, X. Xu, J. F. Douglas and W.-S. Xu, *Macromolecules*, 2023, **56**, 4049–4064.
72 T. Desai, P. Keblinski and S. K. Kumar, *J. Chem. Phys.*, 2005, **122**, 134910.
73 S. Peter, H. Meyer and J. Baschnagel, *Eur. Phys. J. E*, 2009, **28**, 147–158.
74 F. W. Starr, S. Sastry, J. F. Douglas and S. C. Glotzer, *Phys. Rev. Lett.*, 2002, **89**, 125501.
75 A. Widmer-Cooper and P. Harrowell, *Phys. Rev. Lett.*, 2006, **96**, 185701.
76 A. Ottochian and D. Leporini, *J. Non-Cryst. Solids*, 2011, **357**, 298–301.
77 L. Larini, A. Ottochian, C. De Michele and D. Leporini, *Nat. Phys.*, 2008, **4**, 42–45.
78 F. Puosi and D. Leporini, *J. Chem. Phys.*, 2012, **136**, 164901.
79 D. S. Simmons, M. T. Cicerone, Q. Zhong, M. Tyagi and J. F. Douglas, *Soft Matter*, 2012, **8**, 11455–11461.
80 B. A. Pazmiño Betancourt, P. Z. Hanakata, F. W. Starr and J. F. Douglas, *Proc. Natl. Acad. Sci. U. S. A.*, 2015, **112**, 2966–2971.
81 J. F. Douglas, B. A. Pazmiño Betancourt, X. Tong and H. Zhang, *J. Stat. Mech.: Theory Exp.*, 2016, **2016**, 054048.
82 G. Mahmud, H. Zhang and J. F. Douglas, *Eur. Phys. J. E*, 2021, **44**, 33.
83 J.-H. Hung, T. K. Patra, V. Meenakshisundaram, J. H. Mangalara and D. S. Simmons, *Soft Matter*, 2019, **15**, 1223–1242.
84 D. Ruan and D. S. Simmons, *J. Polym. Sci., Part B: Polym. Phys.*, 2015, **53**, 1458–1469.
85 R. M. Elder, A. L. Forster, A. Krishnamurthy, J. M. Dennis, H. Akiba, O. Yamamuro, K. Ito, K. M. Evans, C. Soles and T. W. Sirk, *Soft Matter*, 2022, **18**, 6511–6516.
86 E. B. Stukalin, J. F. Douglas and K. F. Freed, *J. Chem. Phys.*, 2010, **132**, 084504.
87 Z. Li and W. Xia, *Extreme Mech. Lett.*, 2020, **40**, 100942.
88 C. L. Soles, A. B. Burns, K. Ito, E. P. Chan, J. F. Douglas, J. Wu, A. F. Yee, Y.-T. Shih, L. Huang, R. M. Dimeo and M. Tyagi, *Macromolecules*, 2021, **54**, 2518–2528.
89 W. Zhang, F. W. Starr and J. F. Douglas, *J. Chem. Phys.*, 2021, **155**, 174901.
90 F. Puosi and D. Leporini, *Eur. Phys. J. E*, 2015, **38**, 87.
91 X. Wang, H. Zhang and J. F. Douglas, *J. Chem. Phys.*, 2021, **155**, 204504.
92 X. Xu, J. F. Douglas and W.-S. Xu, *Macromolecules*, 2023, **56**, 4929–4951.
93 C. Jeong, F. W. Starr, K. L. Beers and J. F. Douglas, *Macromolecules*, 2023, **56**, 3873–3883.
94 R. M. Elder, J. W. Andzelm and T. W. Sirk, *Chem. Phys. Lett.*, 2015, **637**, 103–109.
95 X. Wang, W.-S. Xu, H. Zhang and J. F. Douglas, *J. Chem. Phys.*, 2019, **151**, 184503.
96 Z. Yang, X. Xu, J. F. Douglas and W.-S. Xu, *J. Chem. Phys.*, 2024, **160**, 044503.